Precision Engineering 62 (2020) 16–22

Contents lists available at ScienceDirect

Precision Engineering

journal homepage: http://www.elsevier.com/locate/precision

Evaluation of the performance variation of porous air pads on discontinuous surfaces

C. Sanz [a,b,*], P. Morantz [a,d], A.J.G. Lunt [e], P. Shore [a,d], A. Chérif [b], J. Schneider [c], H. Mainaud-Durand [b], N. Steffens [c]

[a] Cranfield University, College Rd, Cranfield, MK43 0AL, UK
[b] CERN, Route de Meyrin, 1217, Meyrin, GE, CH, Switzerland
[c] HEXAGON Metrology GmbH, Siegmund-Hiepe-Str. 2-12, 35578, Wetzlar, DE, UK
[d] National Physical Laboratory, Hampton Road, Teddington, Middlesex, TW11 0LW, UK
[e] Department of Mechanical Engineering, University of Bath, Bath, BA2 7AY, UK

ARTICLE INFO

Keywords:
Air bearing
Accuracy
Control

ABSTRACT

A new high accuracy position measurement system has been developed. It measures the position of a 0.1 mm diameter copper-beryllium wire that informs alignment of energy beams in advanced particle accelerators. This new measurement system employs air pads to provide precision and friction free rotation of a sensor. To enable the measuring system to be positioned over the wire, a slot is required in the measuring device rotor. To optimise the design of this measuring system it was necessary to understand the performance of the air pads as they pass over the gaps (slots) in the rotor. This paper describes modelling and experiments that were performed to gain understanding of air pad performance when encountering such a surface gap. Particularly, an analytical model of the variation of load of a 20 mm × 40 mm porous air pad during the passing of a 1.5 mm wide slotted surface. Subsequent experimentation revealed that the general behaviour of the load variation had been captured effectively. The results of this analysis reveal that air pads of this size can reliably pass above an opening of this size with about 14% reduction in force. The results and the methodology presented in this paper can be used as an effective basis for future designs and studies.

1. Introduction

One of the projects currently under development at the European Organisation for Nuclear Research (CERN) is the Compact Linear Collider (CLIC). This linear collider is being designed to accelerate electrons and positrons from two opposing directions and to focus them into an elliptical collision point of size of 1 nm × 40 nm. In order to facilitate this cross-sectional size, the incident beams need to be aligned with nanoscale precision. As a result, pre-alignment of CLIC's acceleration and focusing optics (otherwise known as elements) are required at the microscale [1].

State-of-the-art measurement techniques are required in order to facilitate the alignment of these large (several metres) devices at the micrometre level. The PACMAN project (Particle Accelerator Component's Metrology and Alignment to the Nanometre scale) was launched at CERN to address this measurement need [2]. This project is based on aligning the functional axis of each of the CLIC elements with respect to external references, called fiducials [3]. To perform this fiducialisation, the first steps consist of using a stretched wire to find the optimal position for the beam. Once successfully positioned, this wire represents the functional axis and facilitates high accuracy positioning using a coordinate measurement machine (CMM). The wire selected for this task has a 0.1 mm diameter and is composed of copper and beryllium, two materials assuring a reduced sag and a sufficient electrical conductivity.

Currently, no measurement system is capable of localising the wire with the sub-micrometric accuracy required for this application. Therefore, a new sensor, named the Shape Evaluating Sensor: High Accuracy & Touchless (SESHAT), has been designed [4].

The principle of the SESHAT is to rotate a chromatic confocal sensor [5] around the wire which appears as a black dot in Fig. 1. Air bearings are located at 3 equiangular positions around the edge of the sensor in order to suspend the rotor and facilitate rotation. At each position NewWay® [6] air bearings of two differing sizes (12 mm × 24 mm and 20 mm × 40 mm) have been employed and placed in an opposing

* Corresponding author. Cranfield University, College Rd, Cranfield, MK43 0AL, UK.
E-mail address: DrClaudeSanz@gmail.com (C. Sanz).

https://doi.org/10.1016/j.precisioneng.2019.10.014
Received 10 April 2019; Received in revised form 25 September 2019; Accepted 25 October 2019
Available online 31 October 2019

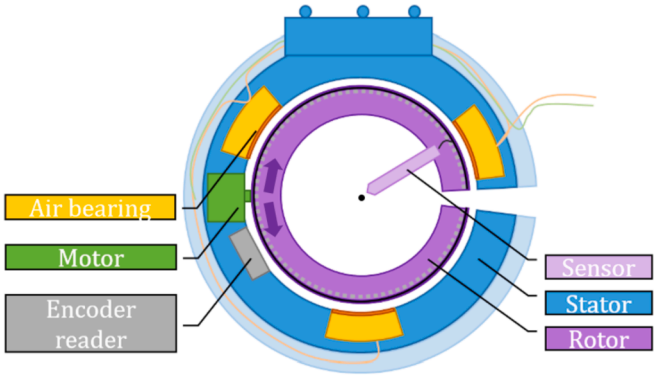

Fig. 1. Schematic of SESHAT design concept. The device is inserted across the wire (shown schematically as a black dot), through the slot, and the rotor moves rotationally relative to the stator in order to measure the form of the wire with microscale precision.

configuration to provide necessary constraint and minimise cross torque, as shown in Fig. 2. The SESHAT employs a piezoelectric actuator which is preloaded against the rotor's surface at all times with a contact stiffness larger than 50 N/μm. Additionally, the SESHAT features a slot in its rotor to allow the stretched wire to pass radially through the bearing assembly to align the sensor to the wire. The focus of this paper is to gain understanding of the influence of this rotor opening on the bearing's performance as its passes into and out of engagement with the air bearings 'active region'.

2. Background

Air pads can provide stiff, stable, reliable, and long lasting bearings with insignificant friction [6]. These characteristics are determined by the quality of the air pads and have been described in detail elsewhere [7]. However, their performance is also based on their assembly (the constraint of the air pad with respect to the bearing surface) and from the use of the appropriate parameters for a specific assembly. For example, the texture and profile of the bearing surface play an important role in the quality of the device. Additionally, the pressurised air must be clean and temperature controlled to assure the bearing's stability.

Previously, the behaviours of air pads with and without porous media have been simulated and compared [8]. These studies have provided arguments both for and against the use of differing air bearing types. The application of a porous intermediate layer has been shown to be tolerable to discontinuity of the bearing surface provided that the vertical offset induced by the discontinuity is smaller than the air gap between the porous media and the bearing surface [6]. Previous studies have also simulated the microstructure of a porous media [9] and finite element optimisation of the air pads' parameters has been performed [10]. Simplified mathematical models can also be used and have been shown to provide comparable predictions of experimental results [11].

A significant amount of research has been performed into the behaviour of air pads that are considerably larger than those required in the SESHAT design [10,12,13]. For these pads, the different air bearing parameters (stiffness, load/lift curve, etc.) have been shown to be proportional to the area over which the pad is acting. In these cases, the load bearing parameters are proportional to the average pressure of the air cushion below an air pad. However, this statement is an approximation and considered inapplicable to the small size air pads necessary for the SESHAT design, due to significant edge effects.

In this paper, an algebraic representation of the air pressure under an air pad with a surface area of several square millimetres is presented. This provides the pressure distribution in order to predict the stiffness evolution of an air pad as it slides across a bearing surface having a slot.

Thereafter, experiments are described which validated the mathematical model as applied to the SESHAT bearings configuration. The prediction of the SESHAT performance is given based on a 1.5 mm size slot. Modelling and experimental measured results are compared.

The motivation for this work has been to provide predictions of the stiffness of the SESHAT's axial 20 mm × 40 mm bearings while two of the six air pads are moving over the rotor's slot. This analysis is crucial to ensure that the stiffness of the system remains above the minimum required by the piezo drive motor at all times. It should be noted that the stiffness in the radial direction does not influence the operation of the SESHAT in the same manner, and therefore simulation and testing of the 12 mm × 24 mm flat air pads was not considered necessary.

3. Method & theoretical results

3.1. Air pressure simulation model

Previous studies have revealed that the air travelling through the pads can be modelled either by a laminar or by a turbulent flow [12]. In the present study, the air flow under consideration arrives at the top of the slot from two different directions: vertically from the porous media and transversally from the air cushions on each side of the air gap, as depicted in figure Fig. 3. Consequently, a turbulent flow model represents more accurately the pressurised air distribution in this system.

During the study, the question of whether the air cushion behaves in the same way when it encounters a slot in the bearing surface or one of the pad's edge arose. The answer was provided by simulations. In order to simulate the air cushion pressure at the edge of the bearing surface of the pads, the software COMSOL Multiphysics 5.2 was used. The air expelled after traversing a porous media was modelled and propagated through the air gap between the air pad and the bearing surface. This simulation was based on a turbulent flow model and a porosity value of 0.17 for the porous media was used [8].

Fig. 4 shows the pressure distribution beneath the pad when the slot in the bearing surface (in black) was at the central position. This result

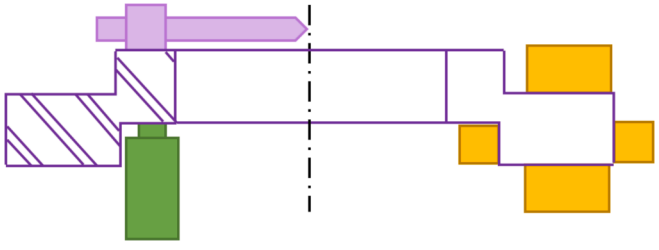

Fig. 2. Schematic drawing of the SESHAT's rotor (in purple) with its rotational axis aligned with the wire during the measurement (shown as a dashed black line). The arrangement of the sensor (in light purple) which is attached to the rotor, four air pads (in yellow) and the piezoelectric actuator (in green) are shown.

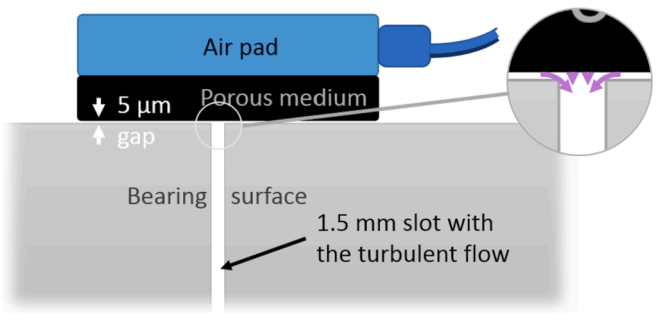

Fig. 3. Schematic side view of the air pad. The air is expelled by the porous media into the 5 μm gap between the air pad and the bearing surface. During the 'slot-passing', some air will be expelled into this channel from the porous media and from the air gap.

demonstrates that there is no significant difference between the air pressure profile at the edge of the porous media (in grey) and that observed close to the edge of the bearing surface (in black). Consequently, these two edge types will be considered as equivalent in the remaining computations. The profile of the air cushion obtained from the simulation result appears in Fig. 5. The nominal air gap of 5 μm and an average nominal air flow of 0.94 NLPM were chosen for the bearing assembly and for the simulations.

3.2. Simulation of load variation above slot

The following computation evaluates the load variation of the pad as it transverses the slot in the bearing surface. In order to perform this analysis, several assumptions were made:

1. The system can be considered to be at equilibrium and the simulation will be based on an instantaneous snapshot of the transition.
2. The stiffness of the bearing surface and air pads are infinite such that the deformations due to applied forces are negligibly small.
3. The line of action of the force on the air pad is at the centre of the air pad's length.
4. The slot is parallel to the air pad's edge and any bevels or imperfections are neglected.
5. The variation of atmospheric air pressure around the pads is negligible such that the relative air pressure on either side of the pads is zero.
6. The dimensions of the air pads and slots are nominally correct such that the dimensional errors have a negligible influence.
7. The pad is mounted on a spherical end screw so that rotation is not influenced by frictional forces.
8. The effect of the bearing surface roughness is negligible such that the model is equally applicable to all of the bearing surface.

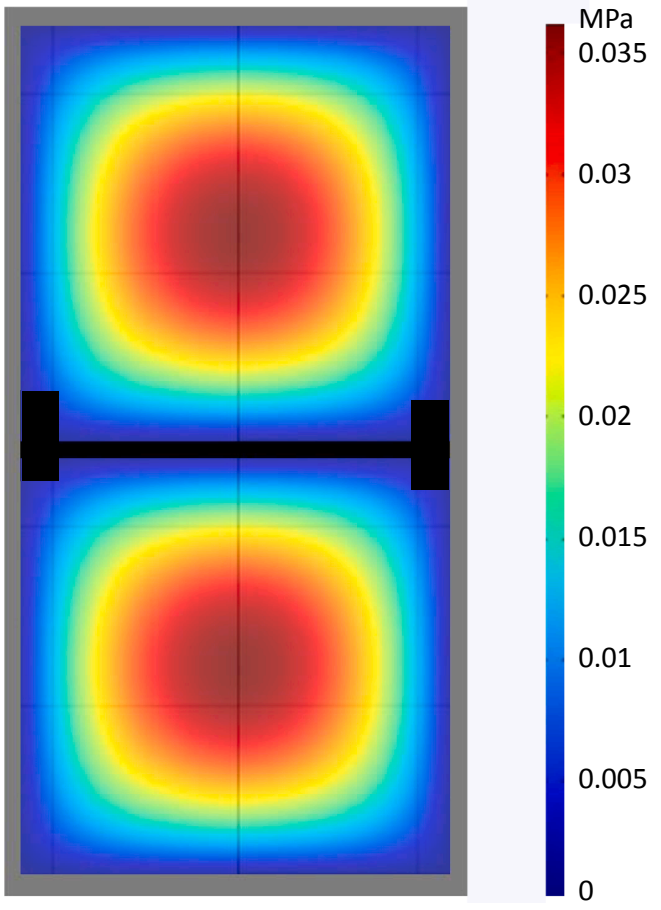

Fig. 4. Simulation result illustrating the behaviour of the air pressure under the porous media of the pad. A similar reduction in pressure is observed at the edge of the pad (grey line) and at the edge of the bearing surface (black line).

The following analysis is based on initially obtaining a mathematical expression for the air pressure as a function of the position under the pad. This expression, in combination with the average air pressure beneath the pad (obtained from the supplier) can then be used to estimate the pressure distribution for a pad above a bearing surface with a slot.

In order to estimate the total load applied to the pad, it can be considered as two smaller pads, on each side of the resisting spherical end screw. For each of the notional pads, the force applied by the air cushion on the pad's surface can be determined by the integral of the pressure distribution over this surface. This force can be expressed as a function of the slot's position and width, in order to provide quantitative estimates for the system.

In order to obtain a generic expression which effectively represents the air pressure under the pads, an expression based on the average pressure beneath the surface of the pad P_{Av} and the distance from the edge of the pad are required. The parameter for position is α. This variable is centered on the axis of symmetry, and is limited within the range $\pm d$ and represents a given distance from the edge of a pad (see Fig. 6). In 1D, an effective representation for the pressure P of a bearing without slot at a given point α can be written as:

$$\mathrm{P}\left(\alpha\right) = 1.1 \times \mathrm{P_{Av}}\left(1 - (\alpha/\mathrm{d})^{10}\right) \tag{1}$$

This equation is defined for the dimensions of a pad with $\mathrm{P_{Av}}$ and d parametrized using the manufacturer's data. If there is a slot reducing the bearing surface to a length λ, then x, replacing α, follows P(α) from zero to the half of the length of the remaining bearing surface, then it follows the same curve reversed:

$$\mathrm{P(x)} = \begin{cases} P(\alpha), x \in [0, \lambda/2] \\ P(\mathrm{d} - \lambda + \alpha), x \in\ ]\lambda/2, \lambda] \end{cases} \tag{2}$$

This resulting pressure distribution is comparable with the simulation results outlined in Section 3.1, as shown in Fig. 5, as well as those observed in previous studies [14]. It should be noted that this analysis was performed on a 12 mm × 24 mm pad, but that this is equally applicable to air pad of any size, including the 20 mm × 40 mm which is

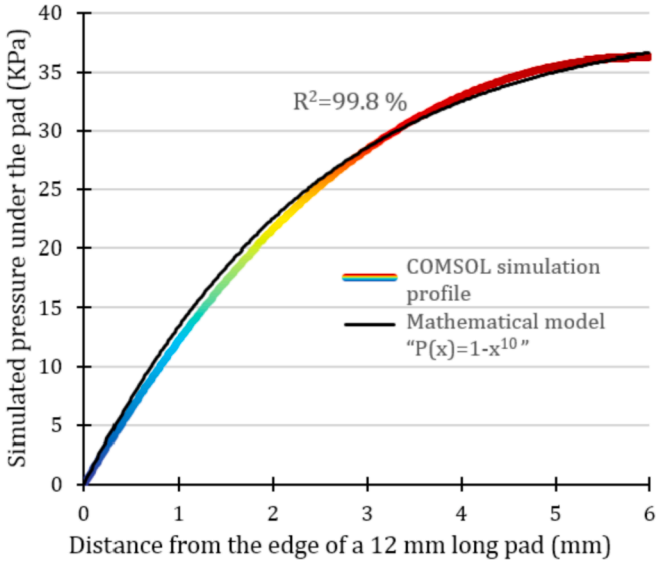

Fig. 5. Comparison between the COMSOL simulation result and proposed model, for a 12 mm long bearing surface under a 24 mm long air pad.

the main focus of this study.

The mathematical model was applied to an air pad with a length d = 24 mm and a maximum pressure without slot $P_{Av} = 38.8$ kPa. Due to the slot, the bearing surface was reduced to a dimension $\lambda = 12$ mm. Thus, the black curve in Fig. 5 shows the curve of equation (1) for $\alpha \in [0, 6]$ – giving the pressure profile of the air cushion from an edge ($\alpha = 0$ mm) to the maximum reached in this configuration (when $\alpha = \lambda/2 = 6$ mm).

This parameterized expression for the variation of pressure can next be used to determine the load variation in the pad as the slot passes beneath the surface. For sake of analysis, the total width of the pad will be written as *w* and the total length as *l*. The pad can be considered in two halves: one to the left of the spherical end screw (in pink in Fig. 6) and one to its right. The pressure distribution can also be considered as two distinct regions: P_I is to the left of the slot (over a distance of $0.5l + s_1$) while P_{II} is to the right of the slot (over a distance $0.5l - s_2$) as shown in Fig. 6 (where the slot appears in red).

The total load lift from the pad F_T, is resisted by the spherical end screw and is equal to the sum of the forces generated by the two sides of the pad (F_{P1} and F_{P2}). For each side, the total reaction force is equal to the integral of the pressure distribution $P(x, y)$ over the cross sectional area (A) of the side:

$$F_{P_n} = \int\int_{A} \mathrm{P(x, y)} \cdot \mathrm{dA}. \tag{3}$$

The expression for $P(x, y)$ can be obtained using 2D formulation of equation (1). Substituting values for the limits in the coordinates x and y shown in Fig. 6, gives the following expressions for the forces of the two sides as a function of the slot position s:

$$F_1(s) = \int_{-0.5l}^{0} \int_{-0.5w}^{0.5w} P_I\,(x_I, y_I) \cdot dy_I \cdot dx_I, \tag{4}$$

$$F_2(s) = \int_{0}^{s_1} \int_{-0.5w}^{0.5w} P_I\,(x_I, y_I) \cdot dy_I \cdot dx_I + \int_{s_2}^{0.5l} \int_{-0.5w}^{0.5w} P_{II}\,(x_{II}, y_{II}) \cdot dy_{II} \cdot dx_{II}, \tag{5}$$

where the subscripts 1 and 2 of the forces refer to the sides 1 and 2. It can be seen that since the width of the pad is constant, the influence of the pressure distribution in the *y* direction can be considered to be constant and an approximation factor k compensating for the integral along y can be used. The force can then be computed using the following expressions which were implemented within a MATLAB function:

$$F_1(s) = k \int_{-0.5l}^{0} P_I\,(x_I) \cdot dx_I, \tag{6}$$

$$F_2(s) = k \left(\int_{0}^{s_1} P_I\,(x_I) \cdot dx_I + \int_{s_2}^{0.5l} P_{II}\,(x_{II}) \cdot dx_{II} \right) \tag{7}$$

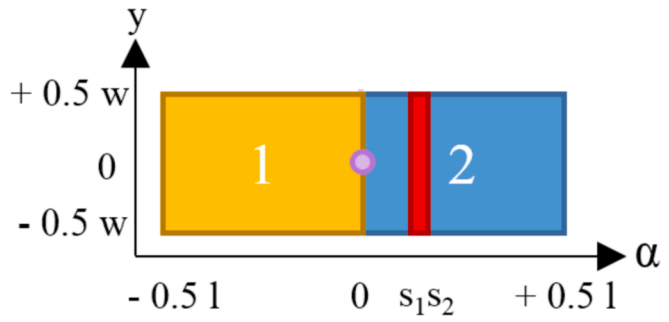

Fig. 6. Top view. The bearing surface of width *w* and length *l* is shown separated into two parts (1 in yellow and 2 in blue). The red region represents the slot which has a thickness of s_2-s_1. The position of the spherical end screw is shown in pink.

3.3. Test bench configuration

In order to validate the model, experimental tests were performed. A 20 mm × 40 mm air pad was arranged to slide in a direction perpendicular to a lapped part which contained a 1.5 mm wide slot. During this process the load generated by the pad was measured. Fig. 7.

The test bench (see Fig. 8 & Fig. 9) was composed of different elements:

- The 20 mm × 40 mm air pad being tested with a temperature controlled (to ± 0.5 °C) air input.
- An aluminium plate featuring a 4 mm deep and 1.5 mm large slot. The two sides were aligned to be parallel, and were produced using lapping to produce a surface with a flatness of 2 μm and a roughness Ra of 0.4 μm.
- A Moore Nanotech 350 UPL turning machine which was used for both pre-alignment and load control at nanoscale precision.
- A Maywoods Instruments U4000 load cell powered by a BST PSA30/3B power supply and read by a Keithley 175 multimetre. The resolution of this setup was 10 μV over a range of 4 mV. Calibration was performed across the expected loading range (0 – 11.5 kg) using a set of known weights prior to the experiment.

The two principal movements used in this experiment are the lathe's X and Z linear axes; the Z axis can be used to change the load applied by the air pad and the X axis can be used to change the relative position of the slot with respect to the air bearing pad. The vacuum holder was used to secure the alum inium plate during the experiment.

In the setup aforementioned, the load measured by the load cell was not equal to the load variation undergone by the air pad. This is due to the limited stiffness of the setup and detailed below.

The acquisition loop was composed of the n elements interacting with the measurement: the Moore machine, the screws and adapters, the load cell and the air pad, with their respective stiffness. The metrological loop was characterised by the stiffness k_{total} such that:

$$k_{total} = \left(\sum_{i=1}^{n} \frac{1}{k_i} \right)^{-1} \tag{8}$$

$$k_{total} = \left(\frac{1}{k_{AirPad}} + \frac{1}{k_{Moore}} + \frac{1}{k_{LoadCell}} + \frac{1}{k_{Screws}} \right)^{-1} \tag{9}$$

For the computation sake, the acquisition loop is divided into two parts: one with a stiffness k_{AirPad} whose variation is to be determined and one with a constant stiffness k_{Setup}, as follows:

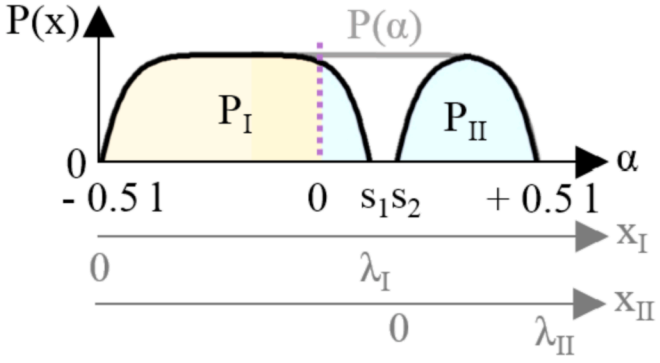

Fig. 7. The pressure distributions P_I and P_{II} are identified. The integral P_1 is shown in light yellow and P_2 in light blue, on each side of the pad's middle (shown as a purple dashed line).

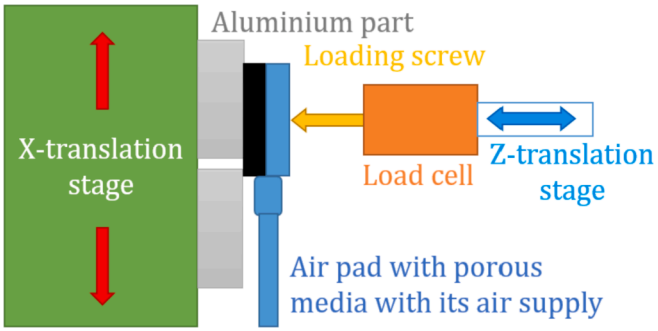

Fig. 8. Schematic of the test bench principle (top view).

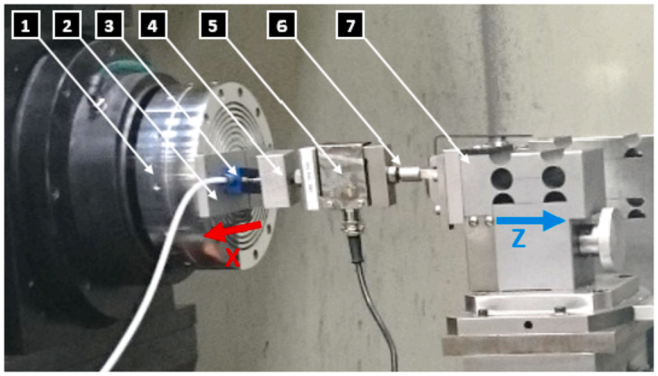

Fig. 9. Overview of the test bench showing key components. (1) The X axis (in red) of the X translation stage of the turning machine (perpendicular to Z, toward the camera that shot the photo). (2) An aluminium plate featuring a 1.5 mm slot which was held onto the translation stage by vacuum. (3) The air pad under test. (4) Adapter between the load cell and air pad loading spherical end screw. (5) The load cell. (6) A screw tightening the load cell and fitting with the machine's holding system. (7) The Z translation stage of the turning machine.

$$k_{total} = \left(\frac{1}{k_{AirPad}} + \frac{1}{k_{Setup}}\right)^{-1},$$
$$\text{with } k_{Setup} = \left(\frac{1}{k_{Moore}} + \frac{1}{k_{LoadCell}} + \frac{1}{k_{Screws}}\right)^{-1}. \quad (10)$$

The force experienced by the pad is defined as the pad's stiffness times Δz, the distance to its resting position:

$$F = k_{total} \cdot \Delta z\ . \quad (11)$$

The resting position is an unknown, as well as Δz. To preload the air pad, Δz increases while z is reduced by the machine's move. When the air pad is preloaded, the machine does not move any longer in the z direction, then z is considered constant and therefore Δz as well (which is true to the parallelism error and the translation uncertainty in the x-direction). As a result, the load is proportional to the stiffness.

When the slot arrives under the air pad, the stiffness k_{AirPad} decreases by a factor γ_{Slot} to $k_{AirPadSlot}$, and thus the spring stiffness k_{total} decreases to $k_{totalSlot}$ such that

$$k_{totalSlot} = \left(\frac{1}{k_{AirPadSlot}} + \frac{1}{k_{Setup}}\right)^{-1}$$
$$k_{totalSlot} = \left(\frac{1}{\gamma_{Slot} \cdot k_{AirPad}} + \frac{1}{k_{Setup}}\right)^{-1}. \quad (12)$$

If we consider the nominal value for the air pad stiffness, an approximated setup stiffness computed from the stiffness of the Moore machine and the load cell (we consider the screws infinitely stiff) and a decrease of 15% due to the slot. The numerical approximation provides the following solutions

$$k_{Setup} = \left(\frac{1}{k_{Moore}} + \frac{1}{k_{LoadCell}} + \frac{1}{k_{Screws}}\right)^{-1}$$
$$k_{Setup} = \left(\frac{1}{50} + \frac{1}{7} + 0\right)^{-1} = 6.1 \text{ N} \Big/ \mu\text{m}, \quad (13)$$

$$k_{total} = \left(\frac{1}{k_{AirPad}} + \frac{1}{k_{Setup}}\right)^{-1} = \left(\frac{1}{14} + \frac{1}{6.1}\right)^{-1}$$
$$k_{total} = 4.3 \ \text{N}/\mu\text{m}, \quad (14)$$

$$k_{totalSlot} = \left(\frac{1}{\gamma_{Slot} \cdot k_{AirPad}} + \frac{1}{k_{Setup}}\right)^{-1}$$
$$k_{totalSlot} = \left(\frac{1}{0.85 \times 14} + \frac{1}{6.1}\right)^{-1} = 4.1 \text{ N} \Big/ \mu\text{m}. \quad (15)$$

In other words, a decrease $\gamma_{Slot} = 15\%$ of the air pad stiffness generates a decrease $\delta = 5\%$ of the stiffness measurement result (thus observable on the load cell acquisition), as expressed below:

$$\delta = \frac{k_{total} - k_{totalslot}}{k_{total}} \times 100 = \frac{4.3 - 4.1}{4.3} \times 100 = 5\% \quad (16)$$

As a result, a correction factor ε must be applied to the total load F_T provided by the mathematical model to compensate for the measurement setup imperfections and determine the final load F_F. It is applied to percentages as follows:

$$F_F = 100 - \varepsilon \cdot (100 - F_T\ ). \quad (17)$$

During the measurement, the setup stiffness is assumed infinite, the load variation measured is thus assumed to result entirely from the air pad stiffness variation. Consequently, for this example, the correction factor ε to be applied to all the measured points has a value of

$$\varepsilon = \frac{100 - F_F}{100 - F_T} = \frac{100 - 95}{100 - 85} = 0.33. \quad (18)$$

Finally, the theoretical maximum stiffness decrease must be corrected by a factor κ resulting from the limited stiffness of the setup, such that

$$\kappa = \frac{F_F - F_T}{F_T} = \frac{95 - 85}{85} = 12\ \ \%. \quad (19)$$

4. Practical results: model validation

4.1. System calibration

Evaluation of the test setup was performed by reproducing the load/lift curve and stiffness curves for the air pad of interest. These curves are provided by the manufacturer [6] for larger air pads, however only one nominal data point had been given for the small air pads used in the SESHAT. In order to populate these curves, the load applied by the pad was incrementally adjusted from 22 N to 169 N (1 mV – 4.5 mV) in 16.3 N steps (0.5 mV). Each air gap was evaluated following several steps:

1) a given force *F* was applied to the air pad without air from the air supply,
2) the readout of the Z-axis was recorded,
3) the air supply was switched on,
4) the machine was translated along its Z-axis until the same force *F* was applied to the air pad,
5) the readout of the Z-axis was recorded again,
6) the change in the Z axis readout was used to approximate the air gap induced by the pad.

The measurement was performed between one and four times for a given load, as shown in Fig. 10.

In order to obtain stiffness estimates s, the load/lift results were differentiated by dividing the change in force by the change in the air gap distance:

$$s(a_n) = \frac{F(a_{n+1}) - F(a_n)}{a_{n+1} - a_n} \quad , \tag{20}$$

where a_n is the air gap thickness at a specific position n and a_{n+1} is the subsequent thickness estimate. Both the stiffness and force F are deemed to be functions of the air gap thickness: when the air gap increases, the stiffness decreases and vice versa.

An identical mathematical treatment to produce the line of best fit in Fig. 10 was performed to obtain the equivalent line given in Fig. 11. Propagation of the error bars was also performed using a similar approach.

4.2. Force variation with pad position

Force variation testing was performed by moving the slot from one end of the air bearing pad to the other end in 1 mm steps. At each position, the force measured by the load cell was logged. This measurement was repeated 6 times, and with two nominally identical air pads. The two air pads data can be observed in Fig. 12.

The tests were performed in a temperature controlled room with a nominal at 20 °C ± 0.5 °C. Nevertheless, a load variation of 1% was seen in the repeatability measurements, which was most likely associated with thermal effects. To minimise this effect, each measurement was performed as soon as the voltmeter of the load cell had stabilised.

Subsequent to the experimental tests the porous graphite air bearing pad surface was inspected and shown not to be damaged. The model was giving a maximum decrease of the stiffness $\gamma_{Slot} = 12.5\%$. It was adjusted to the measurement data (as shown in green in Fig. 12) using a correction factor $\varepsilon = 0.14$. A resulting correction factor due to the limited stiffness of the setup $\kappa = 12\%$ was derived, which matches the theory defined in (19).

5. Discussion

In this report a new analytical model is presented to simulate the response of porous media air pads when the opposing surface contains a slot. Comparison of its results with experimental data has demonstrated this model captures well the behaviour of the pad. However, despite the quality of the correlation, individual data points were found to be noisy in the experimental data set. This noise was associated with the test bench setup. A number of enhancements for future testing include:

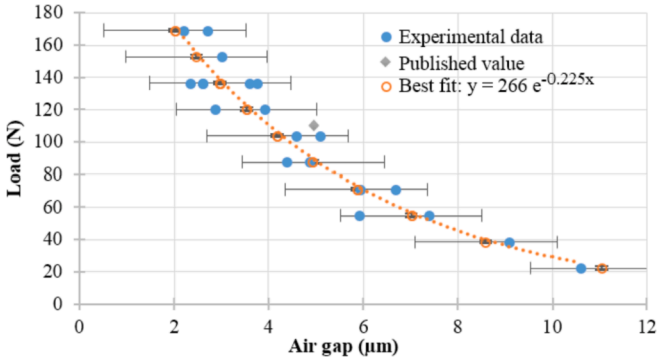

Fig. 10. Lift/Load curve obtained from the 20 mm × 40 mm porous air bearing. The error bars demonstrate the uncertainty of each of the best fit values, which have 99.7% confidence intervals of ± 1 N and ± 1.1 µm, for the load and air gap, respectively.

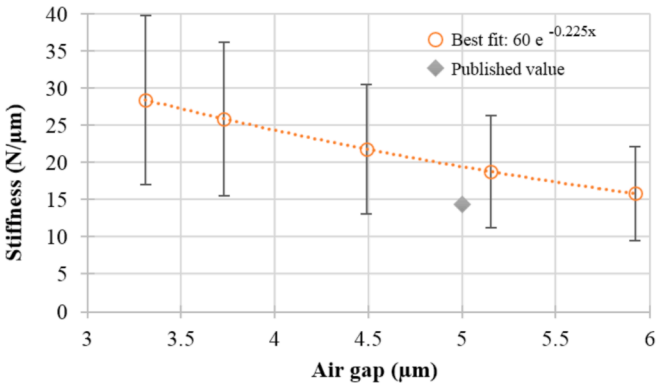

Fig. 11. Stiffness as a function of the air gap for the 20 mm × 40 mm porous air pad. The error bars are derived from those obtained in the lift/load curve.

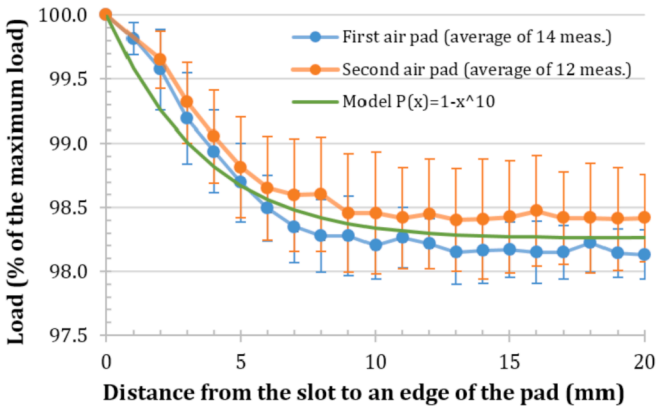

Fig. 12. Static load of a 20 mm × 40 mm air pad as a function of the position of a 1.5 mm large slot sliding below the pad, along its length. The results are expressed as percentages of the maximum load and the errors bars show the 67% confidence intervals.

- A loading spherical end screw could be machined in order to make direct contact with the load cell, thereby reducing the number of interfaces and increasing the mechanical stiffness of the system.
- An automated voltage measurement routine should be implemented to reduce the time to perform measurements. This would reduce the error by facilitating faster measurement protocols and reducing thermal influences and enabling dynamic measurements to be performed.
- An independent displacement sensor should be applied to directly record the air gap, rather than relying on the displacement recorded by the diamond turning machines motions. This will reduce the impact of the error associated with these two measurements.
- The resolution of the load cell (currently 0.4 N), should be improved to enhance the results stability.

Further research on how the stiffness of an air pad is affected by an opening could lead to the self-calibration of the model. This would allow for a generalisation of this model, which would predict load variation for any type of opening in the bearing surface.

This instability of the results illustrates the importance of having an optimised setup to obtain precision with an air bearing. When inserted in an actual mount, the air pads should be in better working conditions than on this test bench and thus, the prediction should describe the load variation obtained with a better precision.

6. Conclusions

A number of different conclusions can be drawn from the results obtained in this article. The first is that 20 mm × 40 mm air pads using state of the art porous graphite media, can be reliably used in nominal conditions above an opening without being damaged. This statement, found in their manufacturer's datasheet [6], is applicable to small air pads.

A model of the load reduction on an air pad while passing a linear opening has been presented and experimentally validated in this paper. The pressure distributions and integration presented has potential for use in a broad range of air pad designs, however calibration of manufacturer specific correction factors are still necessary to make use of this approach. Additionally the lift/load and stiffness curves for the tested 20 mm × 40 mm air pad with porous media are provided with their mathematical expressions.

Concerning the SESHAT design project, the provided model shows that the load variation due to the slot in the bearing surface is not larger than 12.5%. This means that the resulting stiffness remains above the required 50 N/μm at all times. Further simulations will be performed using the results of this analysis in order to determine the impact on the results of the high precision measurement system.

Acknowledgements

We would like to acknowledge the European Union's 7th Framework Programme Marie Skłodowska-Curie actions (grant agreement PITN-GA-2013-606839) and the European Organisation for Nuclear Research who supported this work.

We would like to thank François Morel for the computer-assisted drawing, as well as Claudio Fichera and Federico Carra for their help with the simulations. We would like to extend my thanks to Michaël Guinchard, Alan Heaume, Jacky Tonoli, and Daniel Aubert for their help in experimentation setups. Thanks also go to Solomon Kamugasa, Richard Leach and Byron Knapp for their help in writing the article.

References

[1] Aicheler M. A Multi-TeV linear collider based on CLIC technology: CLIC Conceptual Design Report. Geneva: CERN); 2012.
[2] Caiazza D, Catalan Lasheras N, Mainaud Durand H, Modena M, Sanz C, Tshilumba D, Vlachakis V, Wendt M, Zorzetti S. New solution for the high accuracy alignment of accelerator components. Phys. Rev. Accel. Beams 2017;20.
[3] Bottura L, Buzio M, Pauletta S, Smirnov N. Measurement of magnetic axis in accelerator magnets: critical comparison of methods and instruments. In: Instrumentation and measurement technology conference, 2006. IMTC 2006. Proceedings of the IEEE (IEEE); 2006. p. 765–70.
[4] Sanz C, Cherif A, Mainaud Durand H, Artoos K, Morel F, Morantz P, Shore P, Schneider J, Steffens N. Rotating sensor for new possibilities on Leitz Infinity coordinate measuring machine. In: Euspen 's 16th international conference & exhibition, nottingham, UK , may 201 6 EUSPEN (nottingham); 2016.
[5] Leach RK, Blateyron F. Optical measurement of surface topography vol Chromatic confocal microscoscopy. 2011.
[6] NewWay. NewWayAirBearing-06-012 Application Guide Rev E 2005-01-18 DR mjw.doc - new_way_application_and_design_guide_ Rev_E_2006-01-18.pdf. 2006.
[7] Bhat N, Barrans SM, Kumar AS. Performance analysis of Pareto optimal bearings subject to surface error variations. Tribol. Int. 2010;43. 2240–9.
[8] Fourka M, Bonis M. Comparison between externally pressurized thrust bearings with different orifice and porous feeding systems. Wear 1997;(210):311–7.
[9] Wang Q L, He M, He Y Q and Han J Fractal characteristics of the microstructure for porous graphite Mater. Res. Innov. 19.
[10] Dong C, Zhang C, Wang B, Zhang G. Reducing the dynamic errors of coordinate measuring machines. J Mech Des 2003;125:831.
[11] Plante J-S, Vogan J, El-Aguizy T, Slocum AH. A design model for circular porous air bearings using the 1D generalized flow method. Precis Eng 2005;29. 336–46.
[12] Uhlmann E, Neumann C. Air bearings based on porous ceramic composites. 2006.
[13] Al-Bender F. On the modelling of the dynamic characteristics of aerostatic bearing films: from stability analysis to active compensation. Precis. Eng Times 2009;33. 117–26.
[14] Rasnick WH, Arehart TA, Littleton DE, Steger PJ. Porous graphite air-bearing components as applied to machine tools. Tenn.(USA): Oak Ridge Y-12 Plant; 1974.